IOPscience iopscience.iop.org

Home Search Collections Journals About Contact us My IOPscience

Harmonic response of a class of finite extensibility nonlinear oscillators

This article has been downloaded from IOPscience. Please scroll down to see the full text article.

2011 Phys. Scr. 83 065009

(http://iopscience.iop.org/1402-4896/83/6/065009)

View the table of contents for this issue, or go to the journal homepage for more

Download details:
IP Address: 200.49.224.88
The article was downloaded on 26/05/2011 at 13:05

Please note that terms and conditions apply.

IOP Publishing Physica Scripta
Phys. Scr. **83** (2011) 065009 (12pp) doi:10.1088/0031-8949/83/06/065009

Harmonic response of a class of finite extensibility nonlinear oscillators

M Febbo

Department of Physics, Institute of Physics of the South (IFISUR) and CONICET, Universidad Nacional del Sur, Avda. Alem 1253, 8000 Bahía Blanca, Argentina

E-mail: mfebbo@uns.edu.ar

Received 22 February 2011
Accepted for publication 28 April 2011
Published 25 May 2011
Online at stacks.iop.org/PhysScr/83/065009

Abstract
Finite extensibility oscillators are widely used to simulate those systems that cannot be extended to infinity. For example, they are used when modelling the bonds between molecules in a polymer or DNA molecule or when simulating filaments of non-Newtonian liquids. In this paper, the dynamic behavior of a harmonically driven finite extensibility oscillator is presented and studied. To this end, the harmonic balance method is applied to determine the amplitude–frequency and amplitude–phase equations. The distinguishable feature in this case is the bending of the amplitude–frequency curve to the frequency axis, making it asymptotically approach the limit of maximum elongation of the oscillator, which physically represents the impossibility of the system reaching this limit. Also, the stability condition that defines stable and unstable steady-state solutions is derived. The study of the effect of the system parameters on the response reveals that a decreasing value of the damping coefficient or an increasing value of the excitation amplitude leads to the appearance of a multi-valued response and to the existence of a jump phenomenon. In this sense, the critical amplitude of the excitation, which means here a certain value of external excitation that results in the occurrence of jump phenomena, is also derived. Numerical experiments to observe the effects of system parameters on the frequency–amplitude response are performed and compared with analytical calculations. At a low value of the damping coefficient or at a high value of excitation amplitude, the agreement is poor for low frequencies but good for high frequencies. It is demonstrated that the disagreement is caused by the neglect of higher-order harmonics in the analytical formulation. These higher-order harmonics, which appear as distinguishable peaks at certain values in the frequency response curves, are possible to calculate considering not the linearized frequency of the oscillator but its actual frequency, which is strongly amplitude dependent. On the other hand, for a high value of the damping coefficient or a low value of excitation amplitude, the agreement between numerical and analytical calculations is excellent. For these cases, the system is prevented from exploring large amplitudes of vibration and therefore the nonlinearity is not much evidenced.

PACS number: 05.45.−a

(Some figures in this article are in colour only in the electronic version.)

1. Introduction

Nonlinear oscillators have become over the last few years an active field of research in many areas of physics and engineering. This interest seems to come from the inherent nonlinear behavior of real-world models and from the fact that the dynamic behavior of this type of system is much richer than that of linear systems. For example, among some interesting phenomena unique to nonlinear systems are the well-known jump phenomenon and the fact that the solutions of nonlinear system are affected by initial conditions. The most popular examples of nonlinear oscillators appear when considering a cubic nonlinear stiffness term (Duffing's oscillator [1]) or a quadratic nonlinear damping term

 © 2011 The Royal Swedish Academy of Sciences

(Van der Pol's oscillator [2]). Naturally, a large variety of other types of nonlinearities have been considered throughout the years. Worthy of mention are the works of Gendelman [3], Lee *et al* [4], van Horssen *et al* [5], Kalmár-Nagy and Shekhawat [6] and Ma and Kahraman [7]. Unlike linear systems, where the principle of superposition applies, nonlinear systems are especially hard to solve and no simple closed form solution can be found. However, various approaches have been developed to study them. Among the most salient methods, it is possible to find perturbation methods [8–10], variational approaches [11, 12], parameter expansion [13, 14], decomposition [15, 16], the multiple scale method [2, 17, 18] or harmonic balance-based methods [19, 20]. Among all these methods, the harmonic balance method (HBM) has been turned into the most efficient tool for solving nonlinear problems in which one or two harmonics can be assumed to predominate in the response [19]. Despite the simplicity of the method (to substitute a Fourier series as the proposed solution into the equations of motion and to equate coefficients of the same harmonic components), its range of applicability covers a large variety of model complexities [8].

Recently, finite extensibility nonlinear oscillators (FENOs) have attracted a great deal of attention in the theory of macromolecules, particularly in the theory of polymer dynamics [21] and DNA dynamics [22], and in the simulation of non-Newtonian fluids [23]. For chain models in polymer dynamics, the FENO models represent the physical situation when the macromolecule (considered a large chain of coupled oscillators) is subjected to strong tensile forces (large stretching). For relatively small amplitudes of vibration, these oscillators can be well described by a linear spring connectivity between monomers; however, the description becomes unrealistic when the molecules are highly stretched and the forces are essentially nonlinear. From the large number of ways that may be possible to select to model a finite extensibility oscillator, a finite extensibility nonlinear elastic potential (FENE) [24] is chosen for the title problem. The reason for selecting this type of potential is that it is widely used in computer simulations of polymers to prevent the overstretching of the chains, thus avoiding unphysical conformations. Despite its fundamental importance, we do not know of previous works on the problem, even in one dimension. However, the case of nonpolynomial (quantum) oscillators (NPO) with a saturable nonlinearity (see e.g. [25–27]) is closely related to it but is not the same. The main difference to FENO lies in the fact that the saturable nonlinearity represents a type of softening (nonpolynomial) nonlinearity in NPO, whereas the FENO possesses a hardening one.

The aim of this work is to study a harmonically driven FENO to extract the fundamental characteristics of its nonlinear dynamical behavior. This paper is organized as follows. The first section is devoted to the introduction of the mathematical formulation of the problem. Within this section, the frequency–amplitude and phase–amplitude relations for the steady-state response of the nonlinear system, as well as a stability analysis of the solution, are also presented. Section 2 presents the effect of system parameters on the characteristics of frequency response curves (FRCs) and the calculation of the critical amplitude of the excitation. The numerical results and comparisons between the analytically obtained FRCs and the numerical calculations are presented in section 4. In particular, the effect of higher-order harmonics on the steady-state response of the system for low and high frequencies of excitation is discussed and analyzed. Finally, the concluding remarks are presented and discussed in section 5.

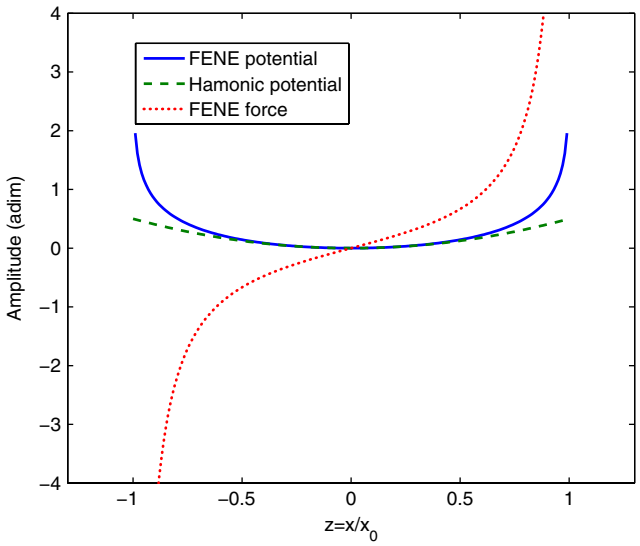

Figure 1. The FENE potential (solid line) and the FENE force (dotted line) as a function of the normalized elongation of the oscillator $z = \frac{x}{x_0}$. For comparison, a harmonic potential is also plotted (dashed line).

2. Mathematical model of the system

One way to model a FENO is, as stated in the introduction, using the FENE potential. Mathematically, it is represented by the following expression:

$$V_{\mathrm{FENE}}(x) = -\frac{1}{2}k_{\mathrm{NL}}x_0^2 \ln\left(1-\left(\frac{x}{x_0}\right)^2\right). \tag{1}$$

Consequently, the force is given by

$$f_{\mathrm{FENE}}(x) = -\frac{\mathrm{d}V(x)}{\mathrm{d}x} = k_{\mathrm{NL}}\frac{x}{1-\left(\frac{x}{x_0}\right)^2}, \tag{2}$$

where x represents the amplitude of the oscillator and x_0 its maximum possible amplitude. Also, k_{NL} accounts for the linear stiffness constant, which is given, from the microscopic theory of polymers, by $k_{\mathrm{NL}} = \frac{3k_{\mathrm{b}}T}{b^2}$, where k_{b} is the Boltzmann constant, T the temperature and b the distance between the monomers of the chain. A graphical representation of the FENE potential and the force is shown in figure 1.

To obtain the harmonic response of the system, an external force of constant amplitude and variable frequency, $F\cos(\omega t)$, is attached to the oscillator. Using the expression for the FENE force $f_{\mathrm{FENE}}(x)$, the equation of motion takes the following form:

$$m\ddot{x} + c\dot{x} + k_{\mathrm{NL}}\frac{x}{1-(x/x_0)^2} = F\cos(\omega t), \tag{3}$$

where the dot indicates differentiation with respect to t, and m and c are the mass and damper constants.

Introducing new variables, $z = \frac{x}{x_0}$, $\omega_{\mathrm{NL}}^2 = \frac{k_{\mathrm{NL}}}{m}$, $\xi = \frac{c}{2m\omega_{\mathrm{NL}}}$ and $f_0 = \frac{F}{mx_0}$, equation (3) takes the final form

$$\ddot{z} + 2\xi\omega_{\mathrm{NL}}\dot{z} + \omega_{\mathrm{NL}}^2 \frac{z}{1-z^2} = f_0 \cos(\omega t). \tag{4}$$

It is clear from the above substitutions that ω_{NL} represents the linearized frequency or the frequency at small amplitudes of vibration.

2.1. Amplitude–frequency and phase–frequency relations

To study the steady-state response of the FENO at the frequency of excitation, the harmonic balance procedure is used [19]. First, a phase shift $t_0 = \frac{\phi}{\omega}$ is introduced that replaces $\cos(\omega t)$ with $\cos(\omega t + \phi)$. Next, an approximate stationary solution of the form $z = Z\cos(\omega t)$ is replaced in equation (4), which gives the following equation for the amplitude and phase:

$$\begin{aligned} &-Z\omega^2\cos(\omega t) + 2\xi\omega_{\mathrm{NL}}\omega Z\sin(\omega t) + \omega_{\mathrm{NL}}^2 \frac{Z\cos(\omega t)}{1 - Z^2\cos(\omega t)^2} \\ &\quad = f_0(\cos(\omega t)\sin(\phi) - \sin(\omega t)\sin(\phi)). \end{aligned} \tag{5}$$

The term of the nonlinear force (FENE force) can be treated in a manageable form if a Taylor's series expansion is used:

$$\frac{x}{1-x^2} = x\sum_{n=0}^{\infty}(x^2)^n. \tag{6}$$

With the help of Euler's formula, de Moivre's formula and Newton's binomial theorem [28], it is not difficult to write $\cos^{2n+1}(\theta)$ as

$$\cos^{2n+1}(\theta) = \sum_{k=0}^{n} a_{n,k}\cos(2n-2k-1)(\theta), \tag{7}$$

where $a_{n,k}$ is given by

$$a_{n,k} = \frac{1}{2^{2n}}\binom{2n+1}{k}. \tag{8}$$

Substituting equation (7) into (5) and comparing the coefficients of $\cos(\omega t)$ and $\sin(\omega t)$, the following algebraic equations for determining the amplitude Z and the phase ϕ for steady-state harmonic oscillation are obtained:

$$-Z\omega^2 + 2\omega_{\mathrm{NL}}^2 \frac{Z}{\sqrt{1-Z^2} + (1-Z^2)} = f_0\cos(\phi), \tag{9}$$

$$2\xi\omega_{\mathrm{NL}}\omega Z = f_0\sin(\phi), \tag{10}$$

where in equation (9) the identity

$$\sum_{n=0}^{\infty}\binom{2n+1}{n}\left(\frac{Z^2}{4}\right)^n = \frac{2}{\sqrt{1-Z^2} + (1-Z^2)} \tag{11}$$

[28] is used.

From equations (9) and (10), it is possible to obtain the so-called amplitude–frequency relation independent of the phase ϕ. The final equation is found to be

$$Z^2\left(\frac{2\omega_{\mathrm{NL}}^2}{\sqrt{1-Z^2}+1-Z^2} - \omega^2\right)^2 + 4\xi^2\omega_{\mathrm{NL}}^2\omega^2 Z^2 - f_0^2 = 0. \tag{12}$$

Equation (12), together with equations (9) and (10), represents the basis of our further analysis.

2.2. Stability of the steady-state solution

The stability of the solution (in the sense of Lyapunov) can be examined by means of a procedure developed in [19]. This involves substituting $z = Z\cos(\omega t) + u$ for z into equation (4) and keeping the linear terms in the resulting equation. The so-called variational equation leads to, in this case,

$$\begin{aligned} \ddot{u} + 2\xi\omega_{\mathrm{NL}}\dot{u} + \omega_{\mathrm{NL}}^2\Bigg(1 + \sum_{n=1}^{\infty}\frac{2n+1}{2^{2n}}Z^{2n}\Bigg(\binom{2n}{n} + 2\binom{2n}{n-1} \\ \times\cos(2\omega t)\Bigg)\Bigg)u = 0. \end{aligned} \tag{13}$$

Approximating $u = A_1\cos(\omega t) + A_2\sin(\omega t)$ and substituting into equation (13) leads to a system of equations that has a nontrivial solution if the determinant of the matrix coefficients is zero and, in turn, to the equation for obtaining $\omega(Z)$:

$$\begin{aligned} (\omega^2)_{1,2} = &\left(\frac{\omega_{\mathrm{NL}}^2}{(1-Z^2)^{3/2}} - \frac{4\xi^2\omega_{\mathrm{NL}}^2}{2}\right) \pm \\ &\sqrt{\left(\frac{4\xi^2\omega_{\mathrm{NL}}^2}{2} - \frac{\omega_{\mathrm{NL}}^2}{(1-Z^2)^{3/2}}\right)^2 + 4\omega_{\mathrm{NL}}^4} \\ &\times\frac{Z^4(\sqrt{1-Z^2}-3) + Z^2(5-4\sqrt{1-Z^2}) + 2(\sqrt{1-Z^2}-1)}{Z^4(1-Z^2)^{5/2}}. \end{aligned} \tag{14}$$

Equation (14) was obtained using the identities [28]

$$\sum_{n=0}^{\infty}(2n+1)\binom{2n}{n}\left(\frac{Z^2}{4}\right)^n = \frac{1}{(1-Z^2)^{(3/2)}} \tag{15}$$

and

$$\begin{aligned} \sum_{n=0}^{\infty}(2n+1)\binom{2n}{n-1}\left(\frac{Z^2}{4}\right)^n &= \frac{3}{(1-Z^2)^{(3/2)}} \\ &- \frac{2}{(1-Z^2)^{(3/2)}}\frac{1}{Z^2} + \frac{2}{Z^2}. \end{aligned} \tag{16}$$

Summing up, equation (14) defines a curve that forms the boundary between the stable and the unstable solutions.

2.3. Backbone curve and limit envelope

The following discussion reveals several important characteristics of the steady-state response of the FENO when it executes a harmonic motion of frequency ω and amplitude Z.

The study of these characteristics is analyzed using the backbone curve and limit envelope [19].

The backbone curve is defined by equation (9) setting $\cos(\phi) = 0$; this yields

$$\omega^2 = \omega_{\mathrm{NL}}^2 \frac{2}{\sqrt{1 - Z^2} + (1 - Z^2)}, \tag{17}$$

which physically represents the locus of the peak amplitude. It is interesting to note that the position of the backbone curve (intersection with the ω-axis) is only affected by ω_{NL}, i.e. it comes from the linear term of the restoring force ($Z \ll 1$). The curvature, instead, is modified by the nonlinear restoring force characteristic of the FENO as $Z \to 1$. Additionally, the backbone curve is not altered by damping c or the excitation amplitude F.

The limit envelope is obtained by equation (10) for the extreme value of $\phi = \pi/2$, i.e. $\sin(\phi) = 1$. In this case, it is defined by the following equation:

$$Z = \frac{f_0}{2\xi\omega_{\mathrm{NL}}\omega} = \frac{F}{cx_0\omega}. \tag{18}$$

The limit envelope thus divides the plane (Z, ω) into two regions: one for which $c\omega Z \leqslant F/x_0$ and the other in which the previous inequality is not satisfied. This restricts the value of $Z(\omega)$ (equation (12)), which can lie only in the first region. Thus, the limit envelope constitutes the envelope of all possible response curves that are able to exist up to this limit. It is important to note that at the points of intersection with the backbone curve, the limit envelope and the response curve $Z(\omega)$ have a common tangent (see figures 2(a) and (b)). Additionally, the limit envelope is affected only by damping c and the excitation amplitude F. However, it is invariant under changes of the mass m and the nonlinear parameter ω_{NL} or linearized frequency.

Figures 2(a) and (b) illustrate the basic characteristics of the curves mentioned above as well as provide several examples of FRCs of the amplitude of displacement Z for the FENO. The curves were constructed for fixed values of $F = 1\,\mathrm{N}$, $x_0 = 1\,\mathrm{m}$ and $k_{\mathrm{NL}} = 1\,\mathrm{N\,m^{-2}}$. Figure 2(a) shows the backbone curve for three different values of damping $c = 1/2$, 1 and $2\,\mathrm{Ns\,m^{-1}}$ (setting $m = 1\,\mathrm{kg}$). The fact that the FENO has a maximum elongation ($Z = 1$) bends the backbone curve to the ω-axis and makes it asymptotically approach $Z = 1$. Besides that, different amounts of damping modify the maximum value of the FRCs, as in the linear oscillator, but leave the backbone curve unaltered. Nevertheless, there exists a fundamental difference between the FENO and a linear oscillator, which is evidenced possibly when passing from $c = 1$ to $c = 0.5$. For these parameter values, the oscillator passes from a uni-valued response to a multi-valued response due to its nonlinearity. In this sense, there must be some combinations of the parameters of the FENO that presents this typical behavior. This important situation will be treated in the next section.

On the other hand, figure 2(b) demonstrates how different masses leave the limit envelope unaltered. To this end, three different masses for the FENO are considered: $m = 1/2$, 1 and 2, and the damping is set to $c = 1$. It can be observed that the FRCs change their position over the ω-axis (since

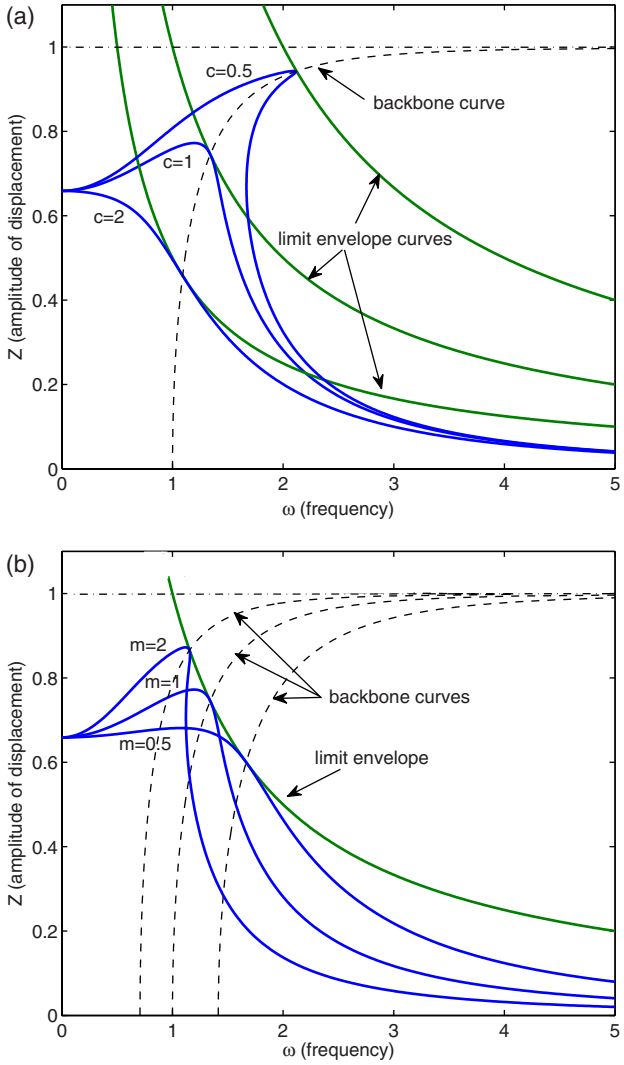

Figure 2. (a) FRCs (solid lines) for the FENO at three different values of damping. (b) The same as (a) but for three different values of the mass.

ω_{NL} changes as well) without altering the limit envelope. Again, a multi-valued response is manifest for $m = 2$. The effect of a maximum elongation is also evidenced for the three cases considered, which causes a bending of the backbone curve towards the ω-axis, making it asymptotically approach $Z = 1$.

3. Effects of system parameters

This section is devoted to the analysis of the effect of the linearized frequency ω_{NL}, the damping coefficient ξ and the excitation amplitude f_0 on the FRCs of Z. As was previously mentioned and observed from figures 2(a) and (b), there exist some combinations of the parameters of the FENO that lead to a multi-valued response for Z.

To investigate this dependence, it is necessary to analyze the roots of the amplitude–frequency relation equation (12). Different multiple real roots lead to a real multi-valued response, whereas complex solutions must be neglected as possible values of Z. A proper treatment of equation (12) that leads to a polynomial of degree ten in Z (or degree five in

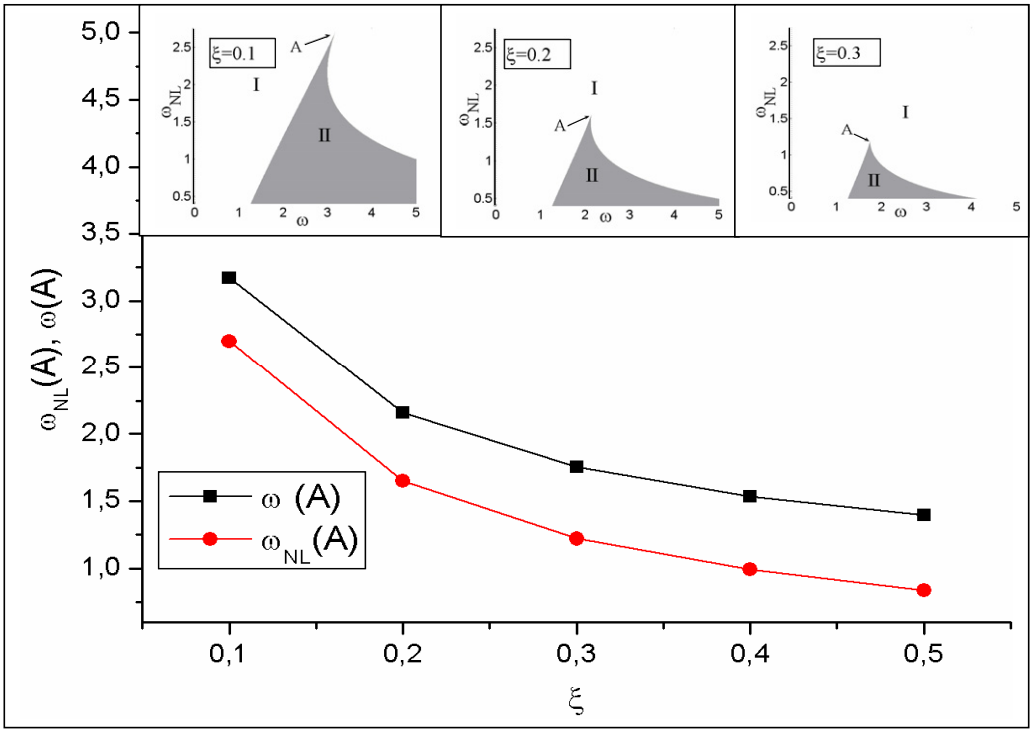

Figure 3. The coordinates of the extreme point A in the (ω, ω_{NL}) plane as a function of damping. The insets show the characteristic regions in the (ω, ω_{NL}) plane for different values of ξ; $f_0 = 1$.

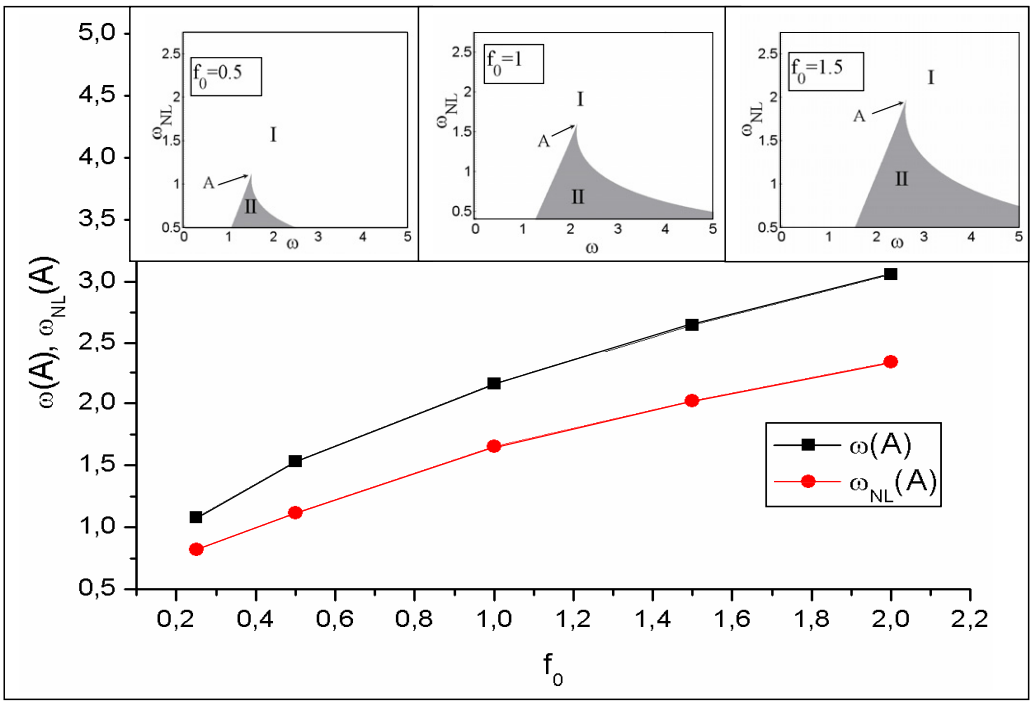

Figure 4. The coordinates of the extreme point A in the (ω, ω_{NL}) plane as a function of excitation amplitude. The insets show the characteristic regions in the (ω, ω_{NL}) plane for different values of f_0; $\xi = 0.2$.

$Y = Z^2$) can be found in appendix A. Generally speaking, no algebraic solution exists for such a quintic equation, and for that reason, one must proceed numerically.

The results of exploring the (ω, ω_{NL}) plane for fixed values of f_0 and ξ can be found in figures 3 and 4, respectively. Additionally, a parametric study of the effect of the variation in these parameters is also presented.

Figure 3 (and inset plots) shows the regions of the (ω, ω_{NL}) plane that leads to a single valued (region I) or a multi-valued (region II) response of the amplitude of displacement Z for different values of ξ (leaving f_0 fixed). The regions are bounded arbitrarily by $0.5 < \omega_{NL} < 2.5$ and $0 < \omega < 5$ for a better presentation of the results. Also, the coordinates of the extreme point A $(\omega(A), \omega_{NL}(A))$ are

plotted as a function of the damping coefficient. From the inset plots, it is possible to appreciate a well-defined separation of the two regions. Region II starts for a value of ω that seems to be independent of the damping and then it grows linearly to A. On the other hand, for $\omega > \omega(A)$ the limit boundary between regions I and II decreases almost like a hyperbola, to meet the ω-axis at a value that depends on damping. More detailed information about the boundary of both regions can be obtained from the plot of the coordinates of the extreme point A. It can be seen that the values of both $\omega(A)$ and $\omega_{\mathrm{NL}}(A)$ decrease, seemingly following an inverse law, as the damping increases. From a physical viewpoint, this implies that having a large value of the damping coefficient, for instance larger than $\xi > 0.3$ (at constant f_0), prevents the system from having a multi-valued response for $\omega_{\mathrm{NL}} > 1.25$ in the whole range of excitation frequencies.

Figure 4 presents the results for the case of varying f_0 at fixed ξ. Qualitatively speaking, this figure presents the same characteristics as those of figure 3. The insets show that a growing value of f_0 makes the extreme point A displace almost over a straight line, increasing the boundaries of region II. Following the same tendency as in figure 3, the limit boundary between regions I and II above $\omega(A)$ decreases almost like a hyperbola and appears to intersect the ω-axis at a value that depends on f_0. Plotting $\omega(A)$ and $\omega_{\mathrm{NL}}(A)$ as a function of f_0 reveals an increment that seems to be nonlinear for increasing values of f_0.

3.1. Critical amplitude of the excitation

The critical amplitude of the excitation means here a certain value of external excitation f_0 that results in the occurrence of jump phenomena in the FRC. Below this critical value, the FRC does not exhibit this typically nonlinear behavior and the system behaves similarly to a linear system. On the other hand, above this limit, a multi-valued response is to be expected for some interval $\omega_- < \omega < \omega_+$ in the FRC. From a physical viewpoint, it is important to obtain this critical amplitude since it represents the limit above which two steady-state solutions are possible with the initial conditions determining which of these represent the actual response of the system.

In order to obtain the critical amplitude, one must first look at the locations of vertical tangency of the FRC. These locations can be obtained by differentiating the amplitude–frequency relation equation (12) implicitly with respect to Z^2 and then setting $\mathrm{d}\omega/\mathrm{d}Z^2 = 0$. The resulting expression is

$$\left(\frac{2\omega_{\mathrm{NL}}^2}{\sqrt{1-Z^2}+1-Z^2}-\omega^2\right)^2+2Z^2\omega_{\mathrm{NL}}^2 \times\left(\frac{2\omega_{\mathrm{NL}}^2}{\sqrt{1-Z^2}+1-Z^2}-\omega^2\right)\frac{(2+(1-Z^2)^{-1/2})}{(\sqrt{1-Z^2}+1-Z^2)^2} +4\xi^2\omega_{\mathrm{NL}}^2\omega^2=0 \tag{19}$$

with the solutions being

$$\omega_\pm(Z)=\omega_{\mathrm{NL}}\sqrt{b(Z^2,\xi^2)\pm\sqrt{b^2(Z^2,\xi^2)-4c(Z^2)}}, \tag{20}$$

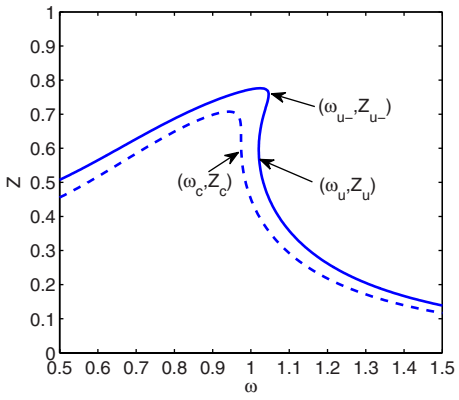

Figure 5. Different FRCs to show the critical amplitude of the excitation as calculated using $(\omega_{\mathrm{u}}, Z_{\mathrm{u}})$, which differs from the correct value $(\omega_{\mathrm{c}}, Z_{\mathrm{c}})$. Data are plotted using $\xi = 0.2$, $\omega_{\mathrm{NL}} = 0.75$.

where

$$b(Z^2,\xi^2)=\frac{2}{\sqrt{1-Z^2}+1-Z^2}+\frac{Z^2(2+(1-Z^2)^{-1/2})}{(\sqrt{1-Z^2}+1-Z^2)^2}-2\xi^2;$$

$$c(Z^2)=\frac{((1-Z^2)^{-1/2}+1+Z^2)}{(\sqrt{1-Z^2}+1-Z^2)^3}.$$

Equation (20) gives, in general, two solutions ω_- and ω_+ that provide the locations of vertical tangency in the FRC for two values of Z: Z_-, Z_+ (see figure 5). The standard procedure to obtain $f_{0\mathrm{crit}}$ (see e.g. [31]) consists in equating $b^2(Z^2,\xi^2) - 4c(Z^2) = 0$, since in this case the two solutions $\omega_\pm$ shrink to one. We name this unique solution as $\omega_{\mathrm{u}} = \omega_{\mathrm{NL}}\sqrt{b(Z^2,\xi^2)}$. Then, Z_{u} is obtained after solving $b^2(Z^2,\xi^2) - 4c(Z^2) = 0$. Unfortunately, it is not possible to give a closed analytical form of Z_{u}, since the resulting polynomial is of ninth degree in Z^2. Finally, substituting ω_{u} and Z_{u} into equation (12), one should be finding the desired result $f_{0\mathrm{crit}}$. However, this is not the correct result for $f_{0\mathrm{crit}}$ as can be observed in figure 5 with the $f_{0\mathrm{crit}}$ calculated from the pair $(\omega_{\mathrm{u}}, Z_{\mathrm{u}})$, $f_{0\mathrm{crit}}$, and the one calculated from the pair $(\omega_{\mathrm{c}}, Z_{\mathrm{c}})$, $f_{0\mathrm{crit}}$, using the procedure given below (we set $\xi = 0.2, \omega_{\mathrm{NL}} = 0.75$ arbitrarily). To qualitatively understand the reason for this discrepancy, one must first plot the amplitude–frequency relation (12) as a function of both ω and Z, replacing for ω each of the two expressions $\omega_+(Z)$ and $\omega_-(Z)$ (equations (20)). After doing this, we will obtain $h_+(Z)$ and $h_-(Z)$ which correspond to the locations of vertical tangency (see equation 12). These functions have the following form:

$$h_\pm(Z)=Z^2\left(\frac{2\omega_{\mathrm{NL}}^2}{\sqrt{1-Z^2}+1-Z^2}-\omega_\pm(Z)^2\right)^2 +4\xi^2\omega_{\mathrm{NL}}^2\omega_\pm(Z)^2Z^2$$

which are plotted in figure 6. It can be seen from this figure that the value of $f_{0\mathrm{crit}}^{(\mathrm{u})}$ calculated above, gives two values of vertical tangency, namely Z_{u} and $Z_{\mathrm{u}-}$ (and ω_{u}, $\omega_{\mathrm{u}-}$) in the FRC which certainly do not correspond to the correct value observed in figure (5). Instead, the correct value of the critical amplitude $f_{0\mathrm{crit}}$ lies in the minimum of the curve $h_-(Z)$ which certainly provides the correct pair of values of $(\omega, Z) = (\omega_{\mathrm{c}}, Z_{\mathrm{c}})$. After substituting them into equation (12),

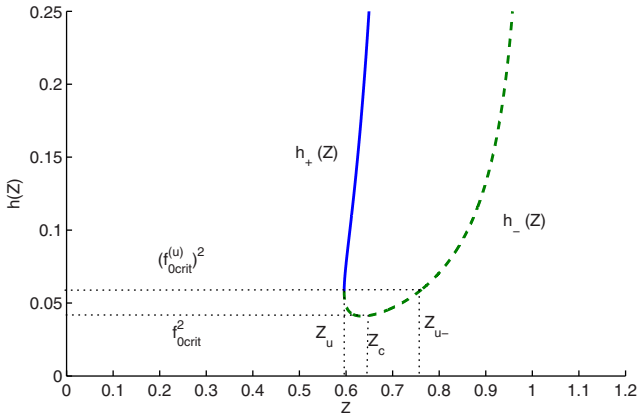

Figure 6. The functions $h_+(Z)$ and $h_-(Z)$ which represent the loci of vertical tangency of the FRC for $\xi = 0.2$, $\omega_{NL} = 0.75$. It is shown that for $f^{(u)}_{0crit}$ there are still two points of Z, Z_u and Z_{u-}, that give vertical tangency of the FRC. On the other hand, for f_{0crit}, only one value of Z, Z_c, satisfies this condition.

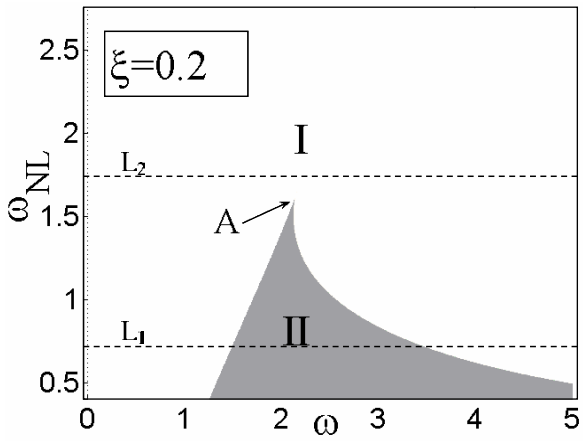

Figure 7. Characteristic regions $L_1 : \omega_{NL} = 0.75$ and $L_2 : \omega_{NL} = 1.75$ where the FRCs of the amplitude of displacement Z exhibit different shapes, for $\xi = 0.2$ and $f_0 = 1$.

one obtains

$$f_{0crit} = \sqrt{Z_c^2\left(\frac{2\omega_{NL}^2}{\sqrt{1-Z_c^2}+1-Z_c^2} - \omega_c^2\right)^2 + 4\xi^2\omega_{NL}^2\omega_c^2 Z_c^2} \tag{21}$$

which gives the critical amplitude of the excitation in terms of the parameters of the problem ξ, ω_{NL}.

4. Frequency response curves and numerical comparisons

It is the aim of this section to present the FRCs for some selected values of ξ and f_0 in order to study the regions of single- and multi-valued responses (I and II) and compare them with numerical calculations. Figure 7 presents the (ω, ω_{NL}) plane for a fixed value of $\xi = 0.2$ and $f_0 = 1$. Lines L_1 ($\omega_{NL} = 0.75$) and L_2 ($\omega_{NL} = 1.75$) are selected to show the shapes of the FRCs for different regions.

Figure 8(a) presents the results for L_1 of the analytically obtained amplitude of displacement Z (solid line) and its

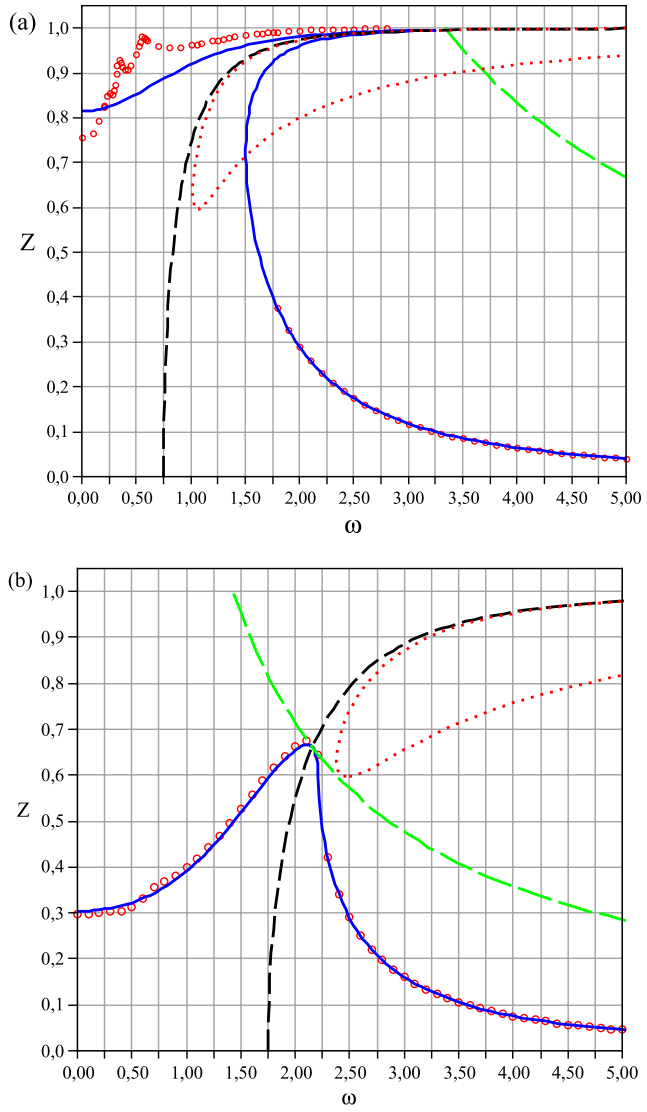

Figure 8. (a) Amplitude of displacement Z for the case L_1 of figure 7 as a function of excitation frequency ω. The analytical solution (solid line), numerical solution (circles), the backbone curve (dashed line), the limit envelope (long dashed line) and the limits of stability (dotted line) are shown. (b) The same as (a) for the case L_2.

numerical counterpart (circles). Also in the same figure, the backbone curve (dashed line), the limit envelope (long dashed line) and the curves that form the boundary of stability, equations (14) (dotted line), are depicted as well. The distinguishable feature in this case is the perfect agreement between both analytical and numerical solutions for the lower branch of the curve and the poor match of both solutions for the upper branch.

To understand qualitatively this behavior, we divide the analysis between the regions of good (upper branch) or poor (lower branch) agreement. Figure 9 shows a typical time domain response and the spectrum obtained at $\omega = 1$ in the region of poor agreement. Clearly, the differences in the results are mainly introduced by ignoring higher-order harmonics in the analytical formulation and appear due to the large amplitude of the oscillation (high stretching). It is interesting to note that only odd harmonics of the excitation frequency ω appear in the response due to the

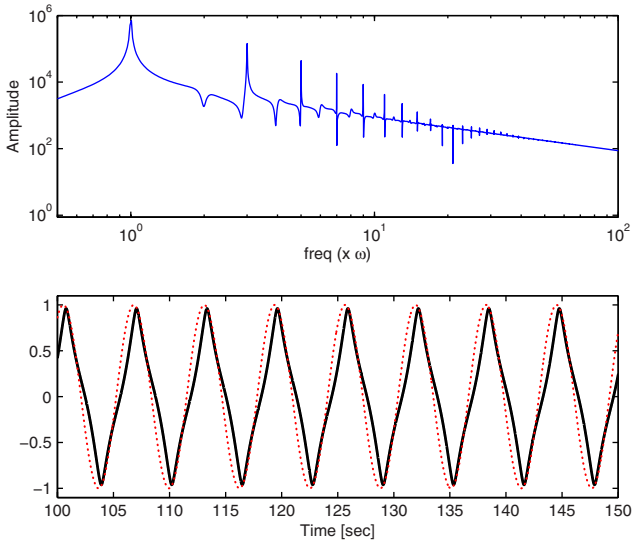

Figure 9. The time domain response and spectrum obtained for L_1 ($\xi = 0.2$, $f_0 = 1$) at $\omega = 1$; solid line, numerical solution. Additionally, a pure cosine function of amplitude 1 is shown for comparison (dotted line).

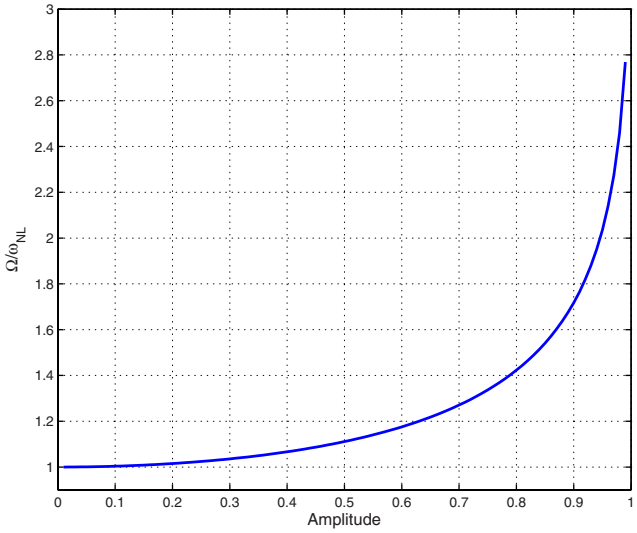

Figure 10. The actual frequency of a FENO as a function of the amplitude of displacement, $\Omega(Z)$, normalized with respect to its value at small amplitudes of vibration ω_{NL}.

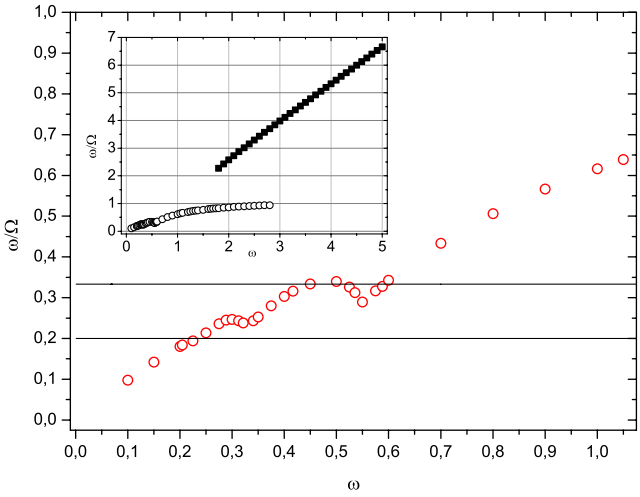

Figure 11. The ratio of the excitation frequency ω to the actual frequency of the FENO, $\Omega(Z)$, versus excitation frequency. The horizontal lines at 1/3 and 1/5 are depicted to indicate the presence of a resonance condition. The inset shows the entire range of excitation frequencies for values of the upper branch of figure 8(a) (white circles) and for values of the lower branch of the same figure (black squares).

characteristics of the nonlinear force $f_{\mathrm{FENE}} \propto \frac{z}{1-z^2} \approx z + z^3 + z^5 + \cdots$. Another distinguishable feature that can be observed in the same figure is that disagreement between the numerical and analytical solutions is more noticeable at low frequencies. It seems that the effect of neglecting higher-order harmonics in the analytical solution is more pronounced for $\omega < 1.5$ than for $\omega > 1.5$. In this sense, in the region of $\omega < 1.5$, two marked peaks are notably distinguished at $\omega \approx 0.34$ and $\omega \approx 0.55$, possibly indicating the existence of resonances. In contrast, for $\omega > 1.5$ both curves approach one another as the amplitude of the response increases to its maximum value ($Z = 1$). It is the aim of the following section to find the reasons for this behavior.

4.1. Effect of higher-order harmonics

The aim here is to capture the essential features of the effect of higher-order harmonics on the FRCs and, at the same time, to provide a qualitative explanation of the appearance of peaks for some particular frequencies. It is a well-known fact [4] that if the excitation frequency ω and the frequency of oscillation of a nonlinear system under the presence of an external force Ω satisfy a resonance condition, i.e.

$$\frac{\omega}{\Omega} = \frac{m}{n}, \quad m, n \text{ integers}, \tag{22}$$

then the amplitude of the system is supposed to be unbounded, limited only by the damping and the nonlinearity. For $m/n = 1$ the system experiences what is called a primary resonance (or main resonance), whereas for $m/n > 1$ a subharmonic or superharmonic, $m/n < 1$, resonance occurs. In most cases [2], it is assumed that the nonlinearity is small and Ω is considered the linearized frequency or frequency at small amplitudes of vibration (ω_{NL} in our case); however, here this is not the case (as we will see later) and we cannot perform the analysis considering ω_{NL} for the resonance condition. Instead, the 'new' frequency Ω, which turns out to be amplitude dependent, has to be used. To find the 'new' Ω we will follow an approximate scheme that consists in calculating the period of the FENO for an undamped free oscillator, as a function of its amplitude of displacement Z. Since we are considering a lightly damped oscillator, the approximation seems to be consistent. Consequently, for the steady-state oscillations, the 'new' frequency Ω is then obtained, giving Z for each different value of the excitation frequency ω.

The exact period for the FENO, as a function of the amplitude of displacement $T(Z)$, was previously calculated in [30] and is given by

$$T(Z) = 4\int_0^Z \frac{\mathrm{d}x}{\sqrt{\ln(G(1-x^2))}}, \tag{23}$$

where the constant G is given by $G = \frac{1}{1-Z^2}$. Unfortunately, $T(Z)$ has no (known) closed analytical form and must be

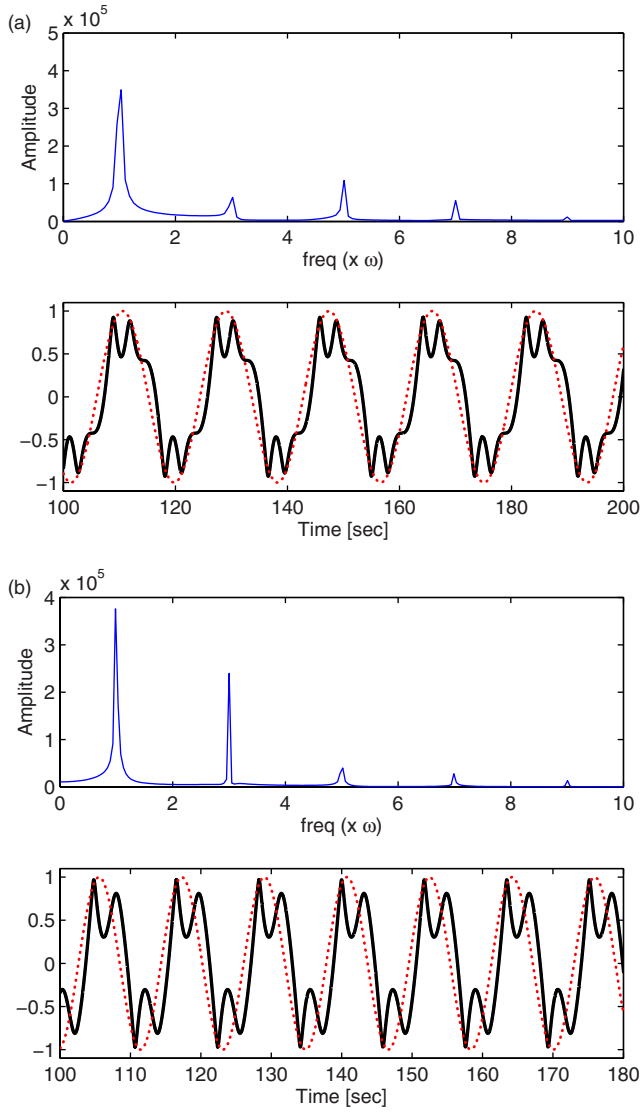

Figure 12. (a) Time domain response and spectrum obtained for L_1 ($\xi = 0.2$, $f_0 = 1$) at $\omega = 0.341$ and (b) at $\omega = 0.538$; solid line, numerical solution; dotted line, a pure cosine function.

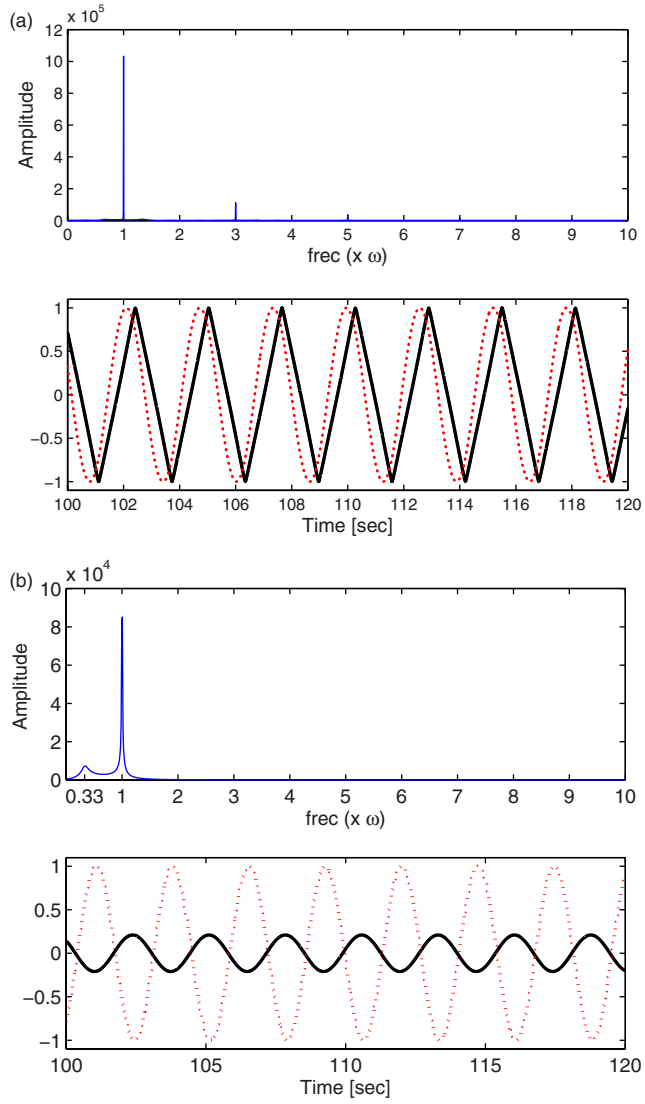

Figure 13. (a) Time domain response and spectrum obtained for L_1 ($\xi = 0.2$, $f_0 = 1$) at $\omega = 2$ for the upper branch of the FRC and (b) at $\omega = 2.3$ for the lower branch of the FRC; solid line, numerical solution; dotted line, a pure cosine function.

numerically calculated. Finally, $\Omega(Z) = \frac{2\pi}{T(Z)}$ is obtained. A graphical representation of the numerically obtained $\Omega(Z)$ normalized with respect to ω_{NL} is shown in figure 10. As was stated before, for $Z > 0.75$, Ω is notably different from ω_{NL} being, for $Z \to 1$, $\omega \ll \Omega \to \infty$. Now, with this result, we are in a position to address the problem of the existence of peaks at some values of excitation frequency. In figure 11, we show the ratio $\omega/\Omega(Z)$ versus ω, where $\Omega(Z)$ is provided by equation (23) for each amplitude Z, numerically determined from figure 8(a) (circles). Recalling that two marked peaks appeared from the FRC for $\omega \approx 0.34$ and $\omega \approx 0.55$, it is expected that some resonance conditions must be satisfied for those frequencies. This is indeed what is shown in figure 11, where a resonance condition $1:3$ ($\omega/\Omega = 1/3$) for $\omega = 0.538$ and another one of the type $1:5$ for $\omega = 0.341$ seem to occur. The cases are confirmed by figures 12(a) and (b) in a time domain response plot and spectrum plot for $\omega = 0.341$ and $\omega = 0.538$, respectively. There, it is possible to see that the third harmonic of the response (which corresponds to $\omega \approx \Omega/3$) is greater than the others for $\omega = 0.538$, and the fifth-harmonic exceeds the others for $\omega = 0.341$ ($\omega \approx \Omega/5$). However, looking carefully at figure 11, the reader may claim that the $1:5$ resonance condition does not match well for $\omega = 0.341$ and matches better for other frequencies, for instance $\omega = 0.225$. Nevertheless, if we look at the spectrum for this frequency, $\omega = 0.225$, it is possible to observe that the fifth harmonic is not predominant in the response and, instead, it is notably smaller than the others. The same happens for $\omega = 0.538$, where the resonance condition is not a 100% match. However, the discrepancies are tolerable taking into account the approximate nature of the determination of Ω and certainly are not to due to the existence of resonance conditions at other frequencies than those shown before.

The situation is rather different for frequencies $\omega > 1.5$. It is observed from figure 8(a) that the match between the analytical and numerical solutions improves as the frequency increases. It is also observed that there is no peak, indicating the absence of a resonance condition, which is confirmed by figure 11 (inset). For these frequencies, a ratio ω/Ω of approximately one clearly indicates the increasing

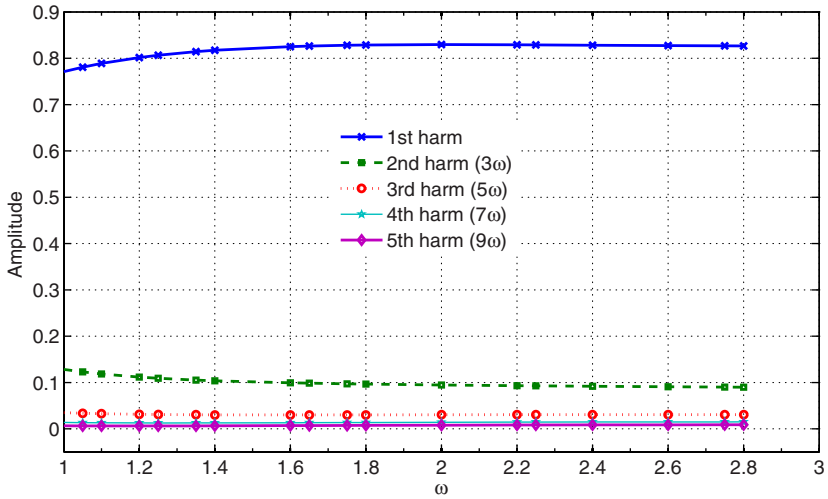

Figure 14. Fourier spectrum (amplitude versus frequency) of the FRCs of case L_1 for the first five harmonics.

importance of the fundamental harmonic in the response. Figure 13(a) shows the time domain response and the Fourier spectrum for $\omega = 2$. There, it is possible to verify that the amplitudes of higher harmonics are negligible compared with the fundamental harmonic (more than ten times larger than the third harmonic, for instance). However, it is the presence of these harmonics that prevents the system from being a pure harmonic motion and, instead, a seemingly triangular function emerges as a result. Therefore, from Fourier analysis, the response can be well approximated by

$$z(t) \approx \sum_{n=\text{odd}} A_0 \frac{1}{n^2} \cos(n\Omega t), \tag{24}$$

which corresponds to a triangular function whose amplitude A_0 in this case is Z dependent. To validate this, figure 14 shows the amplitude of the Fourier components of the time domain response of the forced FENO for frequencies $\omega > 1.5$. The general tendency for all the harmonics is to remain constant as the frequency increases, indicating a frequency independent mathematical description such as the one proposed before. Moreover, the available information gives a ratio of approximately $\left(\frac{n+1}{n}\right)^2$ between A_n and A_{n+1}, which is the one that corresponds to a triangular function, for frequencies higher than $\omega = 2$.

At this point, we have analyzed the region of poor agreement (upper branch of the FRC). It is now the turn of the region of good agreement. If we look at figure 11 (inset, upper arm), we note that Ω is approximately one third the excitation frequency at $\omega = 2.3$; then a subharmonic resonance is expected to occur at this frequency. This fact is evidenced in figure 13(b) from the Fourier spectrum at $\omega = 2.3$. There, it is possible to see a large peak at $\omega = 1$ and another, 10 times smaller peak at $\omega/3$. Since the relative amplitudes between the harmonics is large, it is reasonable to expect, on the one hand, an almost pure harmonic motion of frequency ω for the response of the system, and on the other hand, very good agreement between the analytical and numerical formulations.

Lastly, the FRC corresponding to the line L_2 of figure 7 is shown in figure 8(b). Generally speaking, it can be said that the response of the system resembles that of a linear system. No jump phenomenon and no regions of instability seem to occur for the selected parameters which lead to this particular solution. However, some minor discrepancies are observed at the maximum of the FRC $\omega \approx 2.1$ and at $\omega \approx 0.6$. It is not difficult to see that both discrepancies obey the same reason as before: the fact that higher harmonics are ignored in the analytical formulation. Even in this case, the effect considering higher harmonics produces some differences which are emphasized in the region of the maximum of the curve and at $\omega \approx 0.6$, where a $1:3$ resonance condition occurs $(\omega/\Omega = 1/3)$.

5. Conclusions

In this work, an investigation of a harmonically driven FENO has been presented. The HBM has been applied to determine the amplitude–frequency and amplitude–phase equations. The distinguishable feature in these cases is the bending of the amplitude–frequency curve to the frequency axis, making it asymptotically approach the limit of maximum elongation, $Z = 1$, which physically represents the impossibility of the system reaching this limit. Using the so-called variational equation, the stability condition that defines stable and unstable steady-states solutions has also been derived. Additionally, analytical expressions for the limit envelope curve, which restricts the existence of the steady-state solution to a region of the (Z, ω) plane, as well as for the backbone curve, which represents the locus of the peak amplitude, have also been presented. From the study of the effect of the system parameters on the response, it is possible to conclude that a decreasing value of damping coefficient (ξ) or an increasing value of excitation amplitude (f_0) leads to the appearance of a multi-valued response and the existence of a jump phenomenon. In this sense, the critical amplitude of the excitation, which means here a certain value of external excitation that results in the occurrence of jump phenomena, is also derived. Numerical experiments to observe the effect of the system parameters on the frequency–amplitude response have been performed and compared with analytical calculations. For a low value of damping coefficient or a

high value of excitation amplitude the agreement is poor for low frequencies but good for high frequencies. It has been demonstrated that the disagreement is caused by neglecting higher-order harmonics in the analytical formulation. The effect of higher-order harmonics in the FRCs is numerically studied. They manifest themselves as additional peaks for certain frequencies in the FRCs which satisfy a resonance condition. Then, the values of the peaks can be approximately calculated considering not the linearized frequency of the FENO but its actual frequency, which is strongly amplitude dependent. On the other hand, for a high value of damping coefficient or a low value of excitation amplitude, the agreement between numerical and analytical calculations is excellent. In these cases, the system is prevented from exploring large amplitudes of vibration and, therefore, the nonlinearity is not much evidenced.

Acknowledgments

This study has been sponsored by the Secretaría General de Ciencia y Tecnología of the Universidad Nacional del Sur at the Department of Physics (project no. 24/F050), Agencia Nacional de Promoción Científica y Tecnológica (project PICT 2008-0423) and by CONICET (Argentina). The author is indebted to L M L Alemany for useful comments and very constructive criticism.

Appendix A. Amplitude–frequency equation leading to a polynomial of tenth degree

The amplitude–frequency equation, equation (12), can be put in a more convenient form, getting rid of the radicals. The final expression, which is a tenth degree polynomial on (Z) (after discarding the $Z = 0$ root), $P(Z)$, reads

$$c_{10}Z^{10} + c_8 Z^8 + c_6 Z^6 + c_4 Z^4 + c_2 Z^2 + c_0 = 0, \tag{A.1}$$

with the coefficients, $c_{10}, \ldots, c_0$ (which are functions of $\omega, \omega_{\mathrm{NL}}, \xi, f_0$) given by

$$c_{10} = -\omega^8 - 16\xi^4\omega_{\mathrm{NL}}^4\omega^4 - 8\omega^6\xi^2\omega_{\mathrm{NL}}^2, \tag{A.2}$$

$$\begin{aligned} c_8 = {} & 2\omega^8 + 16\omega^6\xi^2\omega_{\mathrm{NL}}^2 - 8\omega_{\mathrm{NL}}^2\omega^6 - 32\omega_{\mathrm{NL}}^4\omega^4\xi^2 \\ & + 32\xi^4\omega_{\mathrm{NL}}^4\omega^4 + 8\xi^2\omega_{\mathrm{NL}}^2\omega^2 f_0^2 + 2\omega^4 f_0^2, \end{aligned} \tag{A.3}$$

$$\begin{aligned} c_6 = {} & -4\omega^4 f_0^2 + 64\omega_{\mathrm{NL}}^4\omega^4\xi^2 - f_0^4 - 24\omega_{\mathrm{NL}}^4\omega^4 + 16\omega_{\mathrm{NL}}^2\omega^6 \\ & - 32\omega_{\mathrm{NL}}^6\xi^2\omega^2 - 16\xi^2\omega_{\mathrm{NL}}^2\omega^2 f_0^2 - \omega^8 - 8\omega^6\xi^2\omega_{\mathrm{NL}}^2 \\ & - 16\xi^4\omega_{\mathrm{NL}}^4\omega^4 + 8\omega_{\mathrm{NL}}^2\omega^2 f_0^2, \end{aligned} \tag{A.4}$$

$$\begin{aligned} c_4 = {} & 8\xi^2\omega_{\mathrm{NL}}^2\omega^2 f_0^2 + 96\omega_{\mathrm{NL}}^6\xi^2\omega^2 + 2\omega^4 f_0^2 + 40\omega_{\mathrm{NL}}^4\omega^4 \\ & - 32\omega_{\mathrm{NL}}^4\omega^4\xi^2 - 32\omega_{\mathrm{NL}}^6\omega^2 + 8\omega_{\mathrm{NL}}^4 f_0^2 + 2f_0^4 \\ & - 8\omega_{\mathrm{NL}}^2\omega^6 - 16\omega_{\mathrm{NL}}^2\omega^2 f_0^2, \end{aligned} \tag{A.5}$$

$$\begin{aligned} c_2 = {} & -16\omega_{\mathrm{NL}}^8 - f_0^4 + 32\omega_{\mathrm{NL}}^6\omega^2 - 64\omega_{\mathrm{NL}}^6\xi^2\omega^2 - 24\omega_{\mathrm{NL}}^4 f_0^2 \\ & + 8\omega_{\mathrm{NL}}^2\omega^2 f_0^2 - 16\omega_{\mathrm{NL}}^4\omega^4, \end{aligned} \tag{A.6}$$

and the independent term

$$c_0 = 16\omega_{\mathrm{NL}}^4 f_0^2. \tag{A.7}$$

Then, $P(Z)$ can be thought of as a quintic equation in $Z^2 = Y$. As stated by [29] it was first proved by Ruffini (1799) and later by Abel (1826) and Galois (1832) more rigorously that the solutions in radicals to the polynomials of degree five and higher are impossible. This does not mean that there is no algebraic solution to the general quintic equation, but that the existence of such solutions is restricted to a certain type of them. In our case, such an impossibility implies that the roots of equation (A.1) can be obtained only if its coefficients satisfy certain conditions stipulated in [29]. Since it is the aim of the present work to obtain the nature of the roots in all the $\omega, \omega_{\mathrm{NL}}$ planes and not only for the curve defined by such a restriction, this must be done numerically.

References

[1] Virgin L N 1988 On the harmonic response of an oscillator with unsymmetric restoring force *J. Sound Vib.* **126** 157
[2] Nayfeh A H and Mook D T 1979 *Nonlinear Oscillations* (New York: Wiley)
[3] Gendelman O V 2008 Targeted energy transfer in systems with non-polynomial nonlinearity *J. Sound Vib.* **315** 732–45
[4] Lee S-W, Kim J-H and Lee H-W 1997 Relativistic nonlinear dynamics of a driven constant-period oscillator *Phys. Rev.* E **56** 4090–69
[5] van Horssen W T, Pischanskyy O V and Dubbeldam J L A 2010 On the forced vibrations of an oscillator with a periodically time-varying mass *J. Sound Vib.* **329** 721–32
[6] Kalmár-Nagy T and Shekhawat A 2009 Nonlinear dynamics of oscillators with bilinear hysteresis and sinusoidal excitation *Physica* D **238** 1768–86
[7] Ma Q and Kahraman A 2005 Period-one motions of a mechanical oscillator with periodically time-varying, piecewise-nonlinear stiffness *J. Sound Vib.* **284** 893–914
[8] Peng Z K, Lang Z Q, Billings S A and Tomlinson G R 2008 Comparisons between harmonic balance and nonlinear output frequency response function in nonlinear system analysis *J. Sound Vib.* **311** 56–73
[9] Zhu F R and Parker R G 2006 Perturbation analysis of a clearance-type nonlinear system *J. Sound Vib.* **292** 969–79
[10] Thomsen J J and Fidlin A 2003 Analytical approximations for stick-slip vibration amplitudes *Int. J. Non-Linear Mech.* **38** 389–403
[11] Assas L M B 2007 Approximate solutions for the generalized KdV–Burgers' equation by He's variational iteration method *Phys. Scr.* **76** 161–4
[12] Shou D H 2008 Variational approach to the nonlinear oscillator of a mass attached to a stretched wire *Phys. Scr.* **77** 045006
[13] Beléndez A, Pascual C, Álvarez M L, Méndez D I, Yebra M S and Hernández A 2009 Higher order analytical approximate solutions to the nonlinear pendulum by He's homotopy method *Phys. Scr.* **79** 015009
[14] Biazar J and Ayati Z 2008 Application of the Exp-function method to the equal-width wave equation *Phys. Scr.* **78** 045005
[15] Inc M and Cavlak E 2008 On numerical solutions of a new coupled MKdV system by using the Adomian decomposition method and He's variational iteration method *Phys. Scr.* **78** 045008

[16] Ray S S 2007 Exact solutions for time-fractional diffusion-wave equations by decomposition method *Phys. Scr.* **75** 53–61
[17] Cartmell M P, Ziegler S W, Khanin R and Forehand D I M 2003 Multiple scales analyses of the dynamics of weakly nonlinear mechanical systems *Appl. Mech. Rev.* **56** 455–92
[18] Das S K, Ray P C and Pohit G 2007 Free vibration analysis of a rotating beam with nonlinear spring and mass system *J. Sound Vib.* **301** 165–88
[19] Schmidt G and Tondl A 1986 *Non-Linear Vibrations* (Cambridge: Cambridge University Press)
[20] Gottlieb H P W 2004 Harmonic balance approach to periodic solutions of nonlinear jerk equations *J. Sound Vib.* **271** 671–83
[21] Febbo M, Milchev A, Rostiashvili V, Dimitrov D and Vilgis T A 2008 Dynamics of a stretched nonlinear polymer chain *J. Chem. Phys.* **129** 1549081–13
[22] Hatfield J W and Quake S R 1999 Dynamic properties of an extended polymer in solution *Phys. Rev. Lett.* **82** 3548–51
[23] Koplik J and Banavar J R 2003 Extensional rupture of model non-Newtonian fluid filaments *Phys. Rev.* E **67** 011502
[24] Grest G S and Kremer K 1986 Molecular dynamics simulations for polymers in the presence of a heat bath *Phys. Rev.* A **33** 3628–31
[25] Bessis N, Bessis G and Hadinger G 1983 Perturbed harmonic oscillator ladder operators: eigenenergies and eigenfunctions for the $X^2 + \lambda X^2/(1 + gX^2)$ interaction *J. Phys. A: Math. Gen.* **16** 497–512
[26] Handy C R, Hayes H, Stephens D V, Joshua J and Summerour S 1993 Application of the eigenvalue moment method to important one-dimensional quantum systems *J. Phys. A: Math Gen.* **26** 263–59
[27] Saad N, Hall R L and Ciftci H 2006 Study of a class of non-polynomial oscillator potentials *J. Phys. A: Math. Gen.* **39** 7745–56
[28] Gradshteyn I S and Ryzhik I M 1996 *Table of Integrals, Series, and Products* (New York: Academic)
[29] Kulkarni R G 2006 A versatile technique for solving quintic equations *Math. Comput. Education* **40** 205–15
[30] Febbo M 2011 A finite extensibility nonlinear oscillator *Appl. Math. Comput.* **217** 6464–75
[31] Ji J C and Zhang N 2010 Suppression of the primary resonance vibrations of a forced nonlinear system using a dynamic vibration absorber *J. Sound Vib.* **329** 2044–56